Enhanced flame retardancy of rigid polyurethane foam via iron tailings and expandable graphite

Yadong Yang[1], Po Sun[2,*], Junjie Sun[1], Panyue Wen[3], Shihua Zhang[1], Yongchun Kan[3], Xiuyu Liu[1], and Gang Tang[1,*]

[1] School of Civil Engineering and Architecture, Anhui University of Technology, Ma'anshan, Anhui 243032, People's Republic of China

[2] Analysis and Testing Central Facility of Anhui University of Technology, Ma'anshan 243032, People's Republic of China

[3] State Key Laboratory of Fire Science, University of Science and Technology of China, 96 Jinzhai Road, Hefei, Anhui 230026, People's Republic of China

ABSTRACT

To explore the potential application of industrial waste, iron tailings powder, which is in combination with expandable graphite (EG), was adopted to improve the flame retardancy of rigid polyurethane foam (RPUF). The flame retardant performance, combustion performance, and gas products of composites were investigated. The flame retardant test indicated that 20 wt% MITS/EG increased the limiting oxygen index value of RPUF/MITS/EG composite to 23.3–26.6 vol% and passed the V-0. Thermogravimetric analysis test confirmed that MITS/EG improved the overall thermal stability of RPUF-4, and the residual char rate at 700 °C was increased to 35.76 wt%. The peak of heat release rate, total smoke release, and smoke factor of RPUF-4 were reduced by 61.55, 77.99, and 91.54%, respectively, compared with the pure sample, which significantly improved the fire safety of RPUF. Thermogravimetric–Fourier transform infrared spectrometer test implied that MITS/EG system reduced the release intensity of CO_2, isocyanate compounds, and HCN in the composites. Scanning electron microscopy, Raman, and X-ray diffraction tests showed that MITS/EG promoted RPUF to form a heat-resistant and dense expanded char layer.

Introduction

Rigid polyurethane foam (RPUF) is widely used in building insulation, refrigeration, transportation, and other fields due to its excellent thermal insulation performance [1]. However, RPUF without flame retardant treatment is easily ignited and will produce toxic and harmful gases such as hydrogen cyanide, nitric oxide, and carbon monoxide [2–4], resulting in huge economic losses and personnel injuries.

Handling Editor: Jaime Grunlan.

Address correspondence to E-mail: sunpoo@ahut.edu.cn; tanggang@ahut.edu.cn

Therefore, the flame retardant modification of RPUF is particularly necessary [5].

Expandable graphite (EG) is an efficient intumescent flame retardant. Its flame-retardant mechanism is that when EG is heated, the acidic substances between the layers are heated to decompose the acidic gas, promote its own expansion and polymer decomposition, and act as a gas source to promote the formation of expanded char layers, thereby blocking the transport of energy and heat [6]. At present, the flame retardant systems for RPUF flame retardant modification include expandable graphite (EG) [7], pentaerythritol phosphate/EG [8], phosphate/EG [9], ammonium polyphosphate (APP)/EG [10], and Yao et al. [11] investigated the synergistic flame retardant effect of APP and EG in semi-rigid polyurethane foam (SPUF). When the flame retardant content was 20% and the mass ratio of EG/APP was 2:1, the LOI value of the composite was increased by about 51% compared with pure SPUF, 2.9% compared with SPUF/EG, and 16.3% compared with SPUF/APP. The SEM results showed that the residual char after combustion of EG/APP/SPUF was dense, and the microstructure was worm-like.

As a typical solid waste, iron tailings (ITS) are mainly composed of alumina, magnesium oxide, iron oxide, and other oxides, and these metal oxides have been successfully used as polymer fillers [12–15]. Yuan et al. [16] modified $\gamma–Al_2O_3$ on the surface of graphene nanosheets (GO) and introduced it into the polypropylene (PP) matrix to explore the effect of alumina–graphene nanoparticles on PP. The test results showed that the residual char content of PP/$\gamma–Al_2O_3$–GO increased from 0.47–3.85 wt%, and the peak heat release rate (PHRR) decreased by 30.6%. The improvement of flame retardancy was attributed to the barrier effect of graphene and the catalytic char formation of $\gamma–Al_2O_3$ nanosheets.

Based on this, the silane coupling agent was used to modify the surface of ITS, and then, it was compounded with EG to prepare a series of flame retardant rigid polyurethane foam composites in this paper. The thermal stability, combustion characteristics, pyrolysis gas products, and char layer structure of the composites were studied by thermogravimetric (TG), cone calorimeter (CCT), thermogravimetric-infrared (TG-FTIR) and scanning electron microscopy (SEM).

Experimental section

Materials

Polyether polyol (LY-4110; viscosity at 25 °C: 2500 mPa·s; hydroxyl value: 430 mg KOH/g) and triethylenediamine (A33) were bought from Jiangsu Luyuan New Materials Co., Ltd. Polymethylene polyphenyl polyisocyanate (PM200; -NCO content: 30.5–32 wt%; viscosity at 25 °C: 150–250 mPa·s) was purchased from Wanhua Chemical Group Co., Ltd. Silicone oil foam stabilizer (AK8805) was provided by Jining Hengtai Chemical Co., Ltd. Triethanolamine (TEOA) and silane coupling agent (KH550) were purchased by Sinopharm Chemical Reagent Co., Ltd. Catalyst dibutyltin dilaurate (LC) was purchased from Air Products & Chemicals, Inc. Expanded graphite (EG, particle size: 325 mesh, expansion volume: 150 mL/g) was provided by Qingdao Tianhe Graphite Co., Ltd. Iron tailings (ITS; particle size: ≤ 125 um) was kindly supplied by Nanshan Iron Mine in Ma'anshan.

KH550-modified iron tailings

Deionized water (40.0 g) and anhydrous ethanol (160.0 g) were added to a three-neck flask and stirred for 10 min to uniform. Then, the iron tailings (40.0 g) were added to the flask and stirred at 90 °C. After 5 min, KH550 (8.0 g) was added. After 20 min, 5 mL ammonia was added and stirred for 6 h. After filtration and washing, KH550-modified iron tailings (MITS) were obtained by drying at 60 °C.

Preparation of FR-RPUF composites

Table 1 lists the formulation of the RPUF/MITS/EG composites, which were prepared by the one-step water-blown method. According to the ratio in Table 1, reagents other than PM-200 were added to a 500-mL beaker and stirred evenly. Subsequently, PM-200 was added to the mixture and stirred until white and quickly pour into the mold. The sample was cured at 80 °C for 6 h to make the polymerization complete. Finally, the samples were cut into suitable sizes for further characterization.

Table 1 Formulation of RPUF and FR-RPUF composites

Sample	LY-4110/g	PM-200/g	LC/g	AK-8805/g	A33/g	TEOA/g	Water/g	MITS/g	EG/g	MITS/wt%	EG/wt%
RPUF-1	100	135	0.5	2	1	3	2	0	0	0	0
RPUF-2	100	135	0.5	2	1	3	2	60.6	0	20	0
RPUF-3	100	135	0.5	2	1	3	2	40.6	20.3	13.33	6.67
RPUF-4	100	135	0.5	2	1	3	2	30.45	30.45	10	10
RPUF-5	100	135	0.5	2	1	3	2	20.3	40.6	6.67	13.33
RPUF-6	100	135	0.5	2	1	3	2	0	60.6	0	20

Measurement and characterization

Fourier infrared (FTIR): ITS or MITS was mixed with potassium bromide (KBr) in a mortar, and then, the tablet was pressed and tested in Nicolet IS5 infrared spectrometer. The test range was 4000–400 cm^{-1}.

X-ray diffraction (XRD) was employed to analyze the mineral composition of char residue of FR-RPUF composites by D8ADVANCE X-ray diffractometer (Bruker Company, Germany). Test condition: Target material: Cu target; Scanning range: −3–150°; accuracy of goniometer: 0.0001°; 2θ angle accuracy: ≤ 0.02°.

The limiting oxygen index (LOI) was tested by the JF-3 oxygen index analyzer (Nanjing Jiangning Instrument Factory, China) in accordance with ASTM D2863 with a sample dimension of 127 mm × 10 mm × 10 mm.

UL-94 vertical burning test was gained using CZF-3 (Nanjing Jiangning Instrument Factory China) in accordance with ASTM-D3801-2010. The sample size was 127 mm × 13 mm × 10 mm.

Thermogravimetric (TG) was conducted on a Q5000IR thermogravimetric analyzer (TA Instruments, USA). 5–10 mg of sample was heated from room temperature to 800 °C with a heating rate of 20 °C/min. Concerning the thermal analyses of RPUF/MITS/EG formulations, the theoretical TG curves were computed. The theoretical TG curve was computed by a linear combination between the TG curves of RPUF/MIT and RPUF/EG.

$$W_{th}(T)_{[RPUF/MITS/EG]} = x \times W_{exp}(T)_{[RPUF/MITS]} + y \times W_{exp}(T)_{[RPUF/EG]} \quad (1)$$

$$x + y = 1 \quad (2)$$

where $W_{exp}(T)_{[RPUF/MITS]}$: TG curve of the RPUF/MITS; $W_{exp}(T)_{[RPUF/EG]}$: TG curve of the RPUF/EG; x, y were the weight percentages of MITS and EG in RPUF, respectively.

Thermogravimetric–Fourier transform infrared spectrometer (TG-FTIR) was performed using Q5000IR (TA Instruments, USA) thermo-analyzer instrument, which linked to Nicolet 6700 FTIR spectrophotometer (Thermo Scientific Nicolet, USA). 5–10 mg of sample was placed in an alumina tray of the TGA and heated from room temperature to 800 °C at 20 °C /min in a nitrogen atmosphere.

Scanning electron microscope (SEM) was performed to obtain the image of RPUF, FR-RPUF, and composites' char residues by JSM-6490LV scanning electron microscope (JEOL Ltd, Japan). In order to enhance the electrical conductivity of the materials, the samples were coated with a thin conductive layer before observation.

Cone calorimetry was investigated using a conical calorimeter (Fire Testing Technology, UK) in accordance with ISO 5660. The samples with a size of 100 mm × 100 mm × 25 mm were covered with aluminum foil, and the uncovered upper surface was placed horizontally on the sample bench of a cone calorimeter for testing. The thermal radiation flux was set at 35 kW/m^2.

The Raman spectra were used to assess the degree of graphitization of residues on an inVia Reflex Laser Raman spectroscopy (Renishaw, UK) with a wavenumber range set from 800–2000 cm^{-1} and resolution of 1 cm^{-1}.

X-ray photoelectron spectroscopy (XPS) with a VG ESCALAB II spectrometer (Thermo-VG Scientific Ltd USA) using Al Kα excitation radiation (Hv = 1253.6 eV) was used to analyze the char residue of the sample.

Results and discussion

Chemical composition of MITS

Figure 1 shows the infrared spectrum of ITS before and after modification. The peak near 3390 cm^{-1} was attributed to the stretching vibration of –OH of crystal water in iron tailings [17], and the peak at

1430 cm^{-1} corresponded to the characteristic absorption peak of CO_3^{2-} [18]. From the infrared curve of MITS, the absorption peaks at 3620 cm^{-1} and 2920 cm^{-1} were attributed to the N–H and –CH$_2$–stretching vibration peaks on aminopropyl, respectively, and the absorption peak at 1020 cm^{-1} corresponded to the stretching vibration peak of Si–O–Si. The stretching vibration peak of Si–OH at 760 cm^{-1} [19] and the bending vibration peak of Si–O at 463 cm^{-1} were both enhanced, indicating that KH550 successfully modified ITS.

Figure 2 shows the thermogravimetric curves of the iron tailings before and after modification, the weight loss of ITS and MITS at 100–400 °C was
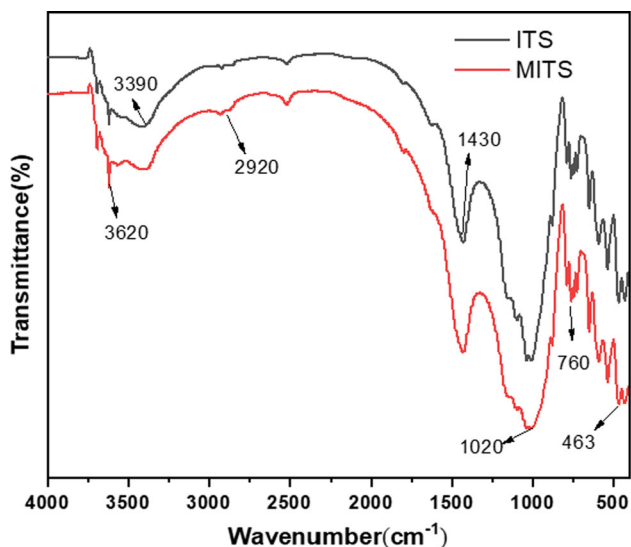
mainly due to the loss of free water and bound water [20], and the weight loss at high temperature was due to the decomposition of carbonate [21]. At the same time, it could be observed that MITS began to lose weight at low temperature and the mass loss was higher than that of ITS, which was mainly due to the decomposition of KH550 on the surface of MITS [22]. Due to the influence of KH550, the maximum weight loss rate of MIT was significantly lower than that of ITS and the T_{max} increased in differential thermogravimetric curve, indicating that KH550 has been successfully coated on the surface of iron tailings.

Mechanical properties

Table 2 provides the density and thermal conductivity of RPUF and FR-RPUF composites. The density of pure RPUF is 64.16 kg/m^3. Since the apparent density of EG (about 200 kg/m^3) was higher than that of the original RPUF, the incorporation of EG led to an increase in the density of RPUF-6, while the apparent density of FR-RPUF samples partially replaced by MITS decreased, but slightly higher than that of pure samples. Thermal conductivity is an important parameter to characterize the thermal insulation performance of composites. The thermal conductivity of pure RPUF is 0.0366 W/(m·K), indicating that it has good thermal insulation performance. The thermal conductivity of RPUF-6 is 0.0393 W/(m·K), because its density is much higher than that of pure sample. In general, the thermal conductivity of RPUF is affected by density, cell size, open cell number, and foaming agent [23]. With the increase of the proportion of MITS, the thermal

Figure 1 FTIR spectrum of iron tailings before and after modification.
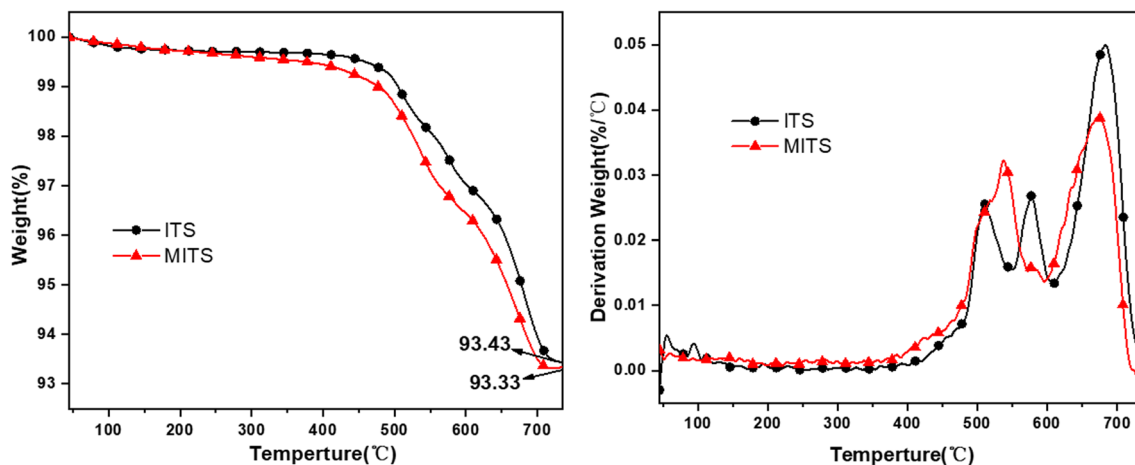
Figure 2 Thermal stability curves of iron tailings before and after modification.

conductivity of FR-RPUF decreases and is lower than that of the pure sample, indicating that MITS and/or EG have little effect on the thermal conductivity of the composites, and the composites still maintain excellent thermal insulation performance.

Morphology

The microstructure of RPUF and FR-RPUF composites was observed by SEM to explore the effect of flame retardant particles on the pore structure of polyurethane. As shown in Fig. 3a, the pure RPUF sample had a closed pore structure with a uniform pore size of 300–400 μm [24]. When 20 wt% MITS was added, the pore size of RPUF-2 became larger but the

uniformity decreased, and the cell also appeared to have certain damage, which was caused by the poor compatibility between MITS and RPUF matrix. When 20 wt% EG was added, the cell uniformity of RPUF-6 also decreased and some penetrating holes appeared, which was mainly due to the incompatibility between EG particles and the RPUF matrix that would penetrate the cell wall and destroy the cell structure [25]. When 20 wt% MITS/EG (m_{MITS}: m_{EG} = 1:1) was added, the damage to RPUF-4 was more serious, which may be due to the superposition of adverse reactions between MITS, EG and RPUF matrix, which further destroyed the cell structure of the composite.

Thermal stability

The effect of MITS/EG on the thermal stability of the RPUF matrix under nitrogen conditions is exhibited in Fig. 4, and the relevant data are listed in Table 3. The results showed that the initial decomposition temperature ($T_{-5wt\%}$) of the pure sample was 273 °C, and the decomposition midpoint temperature ($T_{-50wt\%}$) was 354 °C. The decomposition showed two steps: RPUF hard segment degradation at 250–400 °C and RPUF soft segment degradation at 400–550 °C [26, 27]. The corresponding temperatures (T_{max1} and T_{max2}) of the maximum decomposition rates of the two stages were

Table 2 Mechanical properties of RPUF and FR-RPUF composites

Samples	Density (kg/m^3)	Thermal conductivity (W/(m·K))
RPUF-1	60.4 ± 0.91	0.0366 ± 0.0003
RPUF-2	63.0 ± 2.26	0.0356 ± 0.0004
RPUF-3	63.4 ± 0.57	0.0338 ± 0.0002
RPUF-4	61.3 ± 0.36	0.0347 ± 0.0004
RPUF-5	66.5 ± 0.57	0.0371 ± 0.0004
RPUF-6	95.6 ± 1.64	0.0393 ± 0.0002

Figure 3 SEM images of RPUF and FR-RPUF composites: **a** RPUF-1; **b** RPUF-2; **c** RPUF-4; **d** RPUF-6.
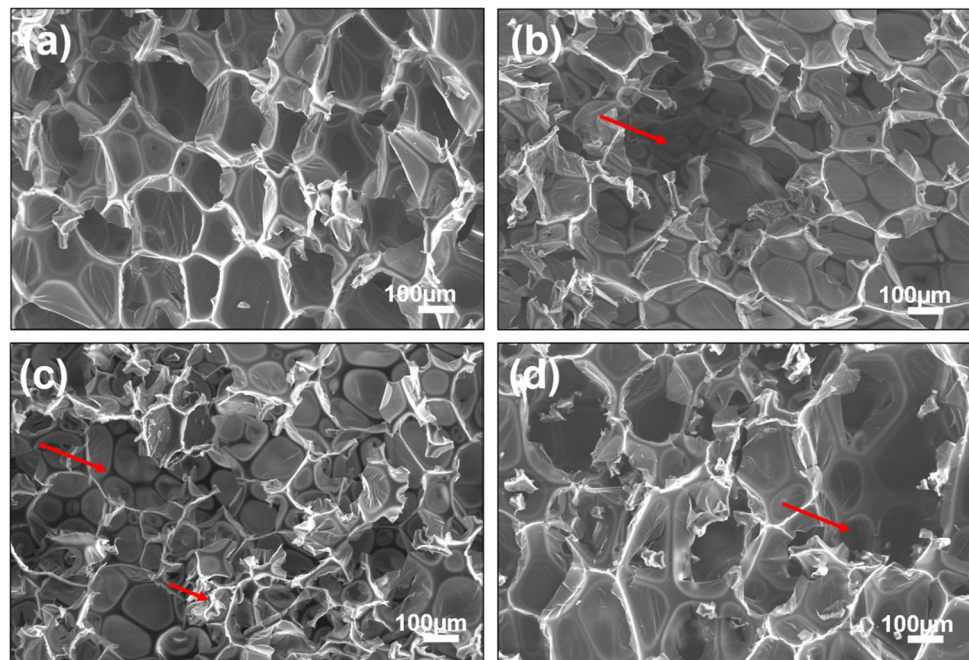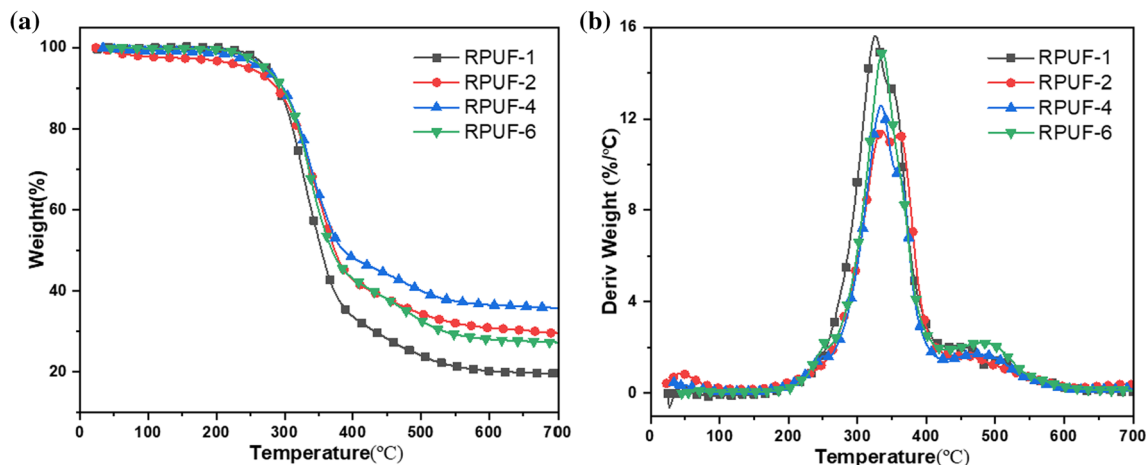
Figure 4 TGA **a** and DTG **b** curves of RPUF and FR-RPUF composites.

Table 3 TG data of RPUF and FR-RPUF composites under N_2 conditions

Sample	$T_{-5wt\%}$(°C)	$T_{-50wt\%}$(°C)	T_{max}(°C)		Char residue at 700 °C (wt%)
			Step1	Step2	
RPUF-1	273	354	323	470	19.56
RPUF-2	246	373	335	464	29.44
RPUF-4	268	386	334	486	35.76
RPUF-6	271	369	336	488	27.28

323 and 470 °C, respectively, and the char residue rate at 700 °C was 19.56 wt%. When 20 wt% MITS was added, the $T_{-5wt\%}$ of RPUF-2 decreased to 246 °C, but the $T_{-50wt\%}$ increased to 373 °C, and the T_{max1} increased to 335 °C compared with the pure sample, indicating that MITS inhibits the degradation of hard segments of polyurethane. The char residue rate at 700 °C was 29.44 wt%, which was caused by MITS promoting polyurethane carbonization and the non-flammable components in MITS. When 20 wt% EG was added, the $T_{-5wt\%}$ of RPUF-6 was almost the same as that of the pure sample, and the $T_{-50wt\%}$, T_{max1}, T_{max2}, and the char residue rate was increased compared with the pure sample. This was because EG formed an expanded char layer that blocked the transport of oxygen and energy and effectively improved the thermal stability of polyurethane composites. When 20 wt% EG/MITS was added, the data of thermal stability were similar to those of RPUF-6 except that $T_{-50wt\%}$ and char residue rate at 700 °C were significantly increased. The char residue rate was 35.76 wt%, which was 82.82% higher than the pure sample, indicating that the combination of EG and MITS effectively improved the high-temperature thermal stability of the composites.
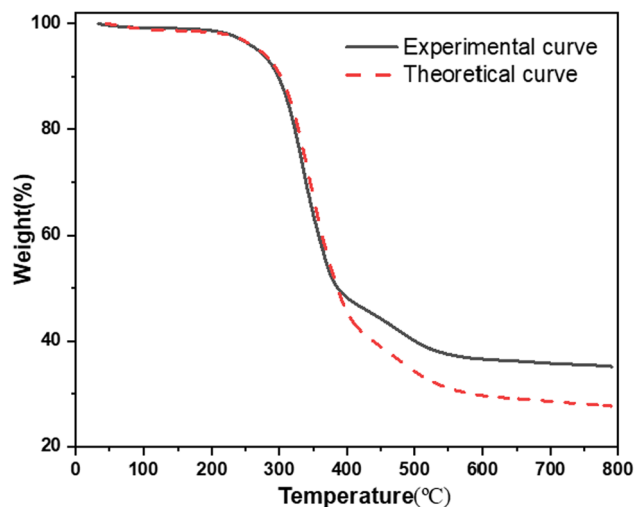

Figure 5 The weight difference between the experimental and theoretical TG curves of RPUF/MIT/EG.

To further investigate the synergistic effect between MITS and EG, Fig. 5 presents the experimental and theoretical TG curves of RPUF-4. If the calculated curve was a linear combination of the TGA curves of the individual components of the system, it meant that there was no synergistic effect between MITS and EG [28]. As shown in Fig. 5, the

experimental curve was always above the theoretical curve, which illustrated that MITS and EG had flame retardant synergistic effect in RPUF composites.

Flame retardant property

The limiting oxygen index (LOI) and vertical combustion (UL-94) were used to evaluate the influence of the MITS/EG system on the flame retardancy of RPUF [29, 30]; the test results are listed in Table 4. The LOI value of RPUF without flame retardant treatment was only 20.1 vol%, and UL-94 was gradeless, so there was a huge potential safety hazard in the use process. When 20 wt% MITS was added, although UL-94 still was gradeless, the molten dripping phenomenon disappeared during the combustion process, and the LOI value increased to 20.7 vol%, indicating that MITS has flame retardancy but the effect was limited. When 20 wt% MITS/EG was added, all RPUF/MITS/EG composites passed UL-94 V-0, and the LOI value also increased significantly (23.3–26.6 vol%). It indicated that MITS and EG had an obvious synergistic effect and effectively reduced the fire risk of RPUF.

In order to further investigate the effect of MITS and EG on the flame retardancy of RPUF, the combustion behavior of RPUF composites was investigated by a cone calorimeter [31, 32]. The cone calorimeter can provide parameters related to heat release and smoke release, including ignition time (TTI), heat release rate (HRR), total heat release (THR), smoke release rate (SPR), total smoke production (TSP) [33]. Figure 6a presents that the TTI of the pure sample was 4 s, HRR reached its peak

Table 4 LOI and UL-94 test results of RPUF and FR-RPUF composites

Sample	LOI/vol%	UL-94		
		t_1/t_2 (s)	Dripping	Rating
RPUF-1	20.1	BC	Y	NR
RPUF-2	20.7	BC	N	NR
RPUF-3	23.3	7.3/0	N	V-0
RPUF-4	24.9	5.8/0	N	V-0
RPUF-5	26.6	1.4/0	N	V-0
RPUF-6	28.8	0.5/0	N	V-0

t_1, t_2—average combustion times after the first and the second applications of the flame; BC—burns to clamp; NR—not rated

(PHRR) which was 442.78 kW/m^2 at 51 s after ignition and then drops to zero at about 150 s. When 20 wt% MITS was added, the HRR curve of RPUF-2 was basically coincident with the pure sample, but the PHRR was slightly lower than the pure sample. When 20 wt% EG or MITS/EG was added, the PHRR of the composites decreased significantly, and the PHRR of RPUF-4 and RPUF-6 decreased by 61.55 and 71.99%, respectively, compared with the pure samples. Figure 6b displays that the THR of RPUF-1 and RPUF-2 rose rapidly at a large slope and then rose slowly to the end at a rate close to the horizontal level. THR of the pure sample was 29.7 MJ/m^2. RPUF-4 and RPUF-6 rose slowly at a relatively small slope, indicating that the addition of EG or MITS/EG could avoid the heat hazard caused by heat accumulation in a short time. The THR of RPUF-4 and RPUF-6 was 27.3 and 23.76 MJ/m^2, respectively.
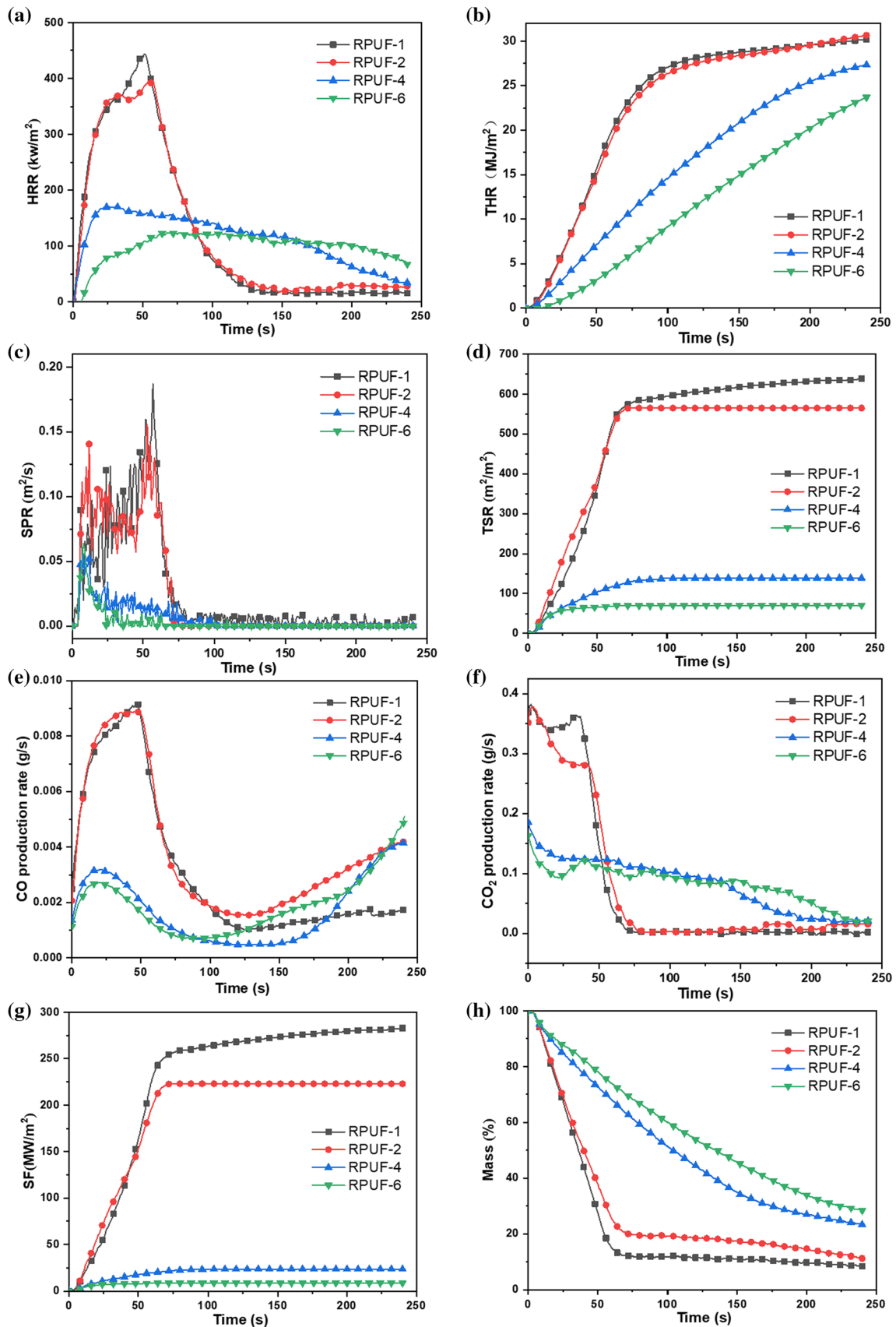
The smoke release rate (SPR) and total smoke release (TSR) were used to characterize the smoke release of the composites during combustion [34, 35]. Figure 6c presents that the SPR curve of the pure sample gradually increased, reached the peak at 57 s, and then rapidly decreased to zero. When 20 wt% MITS was added, the SPR curve peak of RPUF-2 decreased, and the single peak of RPUF-1 changed into double peaks. When 20 wt% EG or MITS/EG was added, the SPR peaks of RPUF-4 and RPUF-6 decreased sharply by 66.02% compared with the pure sample. The TSR of the pure sample was 630.46 m^2/m^2, and the TSR of RPUF-2 decreased to 563.47 m^2/m^2 when 20 wt% MITS was added, indicating that MITS has a certain smoke suppression effect. When 20 wt% EG or MITS/EG was added, the TSR of RPUF-4 and RPUF-6 was significantly reduced, and their values were 138.74 m^2/m^2 and 66.16 m^2/m^2, respectively, which were 77.99% and 89.51% lower than those of the pure samples, illustrating that MITS/EG and EG systems have a significant smoke suppression effect. The smoke parameter (SP) is the product of Av-SEA and PHRR. As can be seen from Table 5, the SP of RPUF-4 and RPUF-6 was much lower than that of the pure sample, showing a good smoke suppression effect.

The smoke factor (SF) is the product of PHRR and TSR [36]; the fire performance index (FPI) is the ratio of TTI to PHRR. The fire growth rate index (FGI) is the ratio of PHRR to the time to reach the peak (T_P), and the three are used to characterize the fire safety of composite materials. The greater the FPI, the

◄ **Figure 6** Characteristic curve of RPUF and FR-RPUF composites: **a** HRR; **b** THR; **c** SPR; **d** TSR; **e** CO production; **f** CO_2 production; **g** SF; **h** mass.

Table 5 Cone calorimetry data of RPUF and FR-RPUF composites

Sample	RPUF-1	RPUF-2	RPUF-4	RPUF-6
TTI (s)	4	5	4	5
T_p (s)	51	54	23	68
PHRR (kW/m^2)	442.78	394.66	170.26	124.05
THR (MJ/m^2)	29.70	31.73	27.33	23.76
TSP (m^2)	6.3	5.63	1.39	0.66
TSR (m^2/m^2)	630.46	563.47	138.74	66.16
Av-EHC (MJ/kg)	30.81	30.13	23.44	27.37
Av-SEA(m^2/kg)	653.88	534.92	122.00	56.72
MLR (g/s·m^{-2})	4.41	3.72	2.22	1.52
CY (wt%)	8.33	11.17	23.32	28.35
FPI (m^2·s/kW)	0.0090	0.0127	0.0235	0.0403
FGI (kW/m^2·s)	8.68	7.31	7.40	1.82
SP (MW/kg)	289.52	211.11	20.77	7.21

Table 6 FRI values calculated in this and other articles

Sample	FRI
RPUF-2	1.31
RPUF-4	2.83
RPUF-6	5.58
RPUF/AHP30 [39]	2.04
RPUF/AHP15/EG15 [39]	2.25
RPUF/EG30 [39]	3.43
RPUF/PA-Al30 [40]	1.26
RPUF-3 [41]	4.18

smaller the SF and FGI, indicating that the smaller the fire risk of the material. It can be seen from Fig. 6g and Table 5 that when MITS/EG or EG was added, the SF and FGI of the composite decreased significantly, which SF of RPUF-6 was about 91.54% lower than that of the pure sample, and FPI increased compared with pure samples, indicating that MITS/EG effectively reduced the fire risk of composites.

As a typical toxic and harmful gas, CO seriously threatens the safety of people in fire [37]. Figure 6e and f presents that the production rates of CO and CO_2 were relatively high after the pure sample was ignited, which was not conducive to the safety of personnel in the fire. Compared with the pure sample, the CO and CO_2 production rates of RPUF-4 decreased sharply in the early stage of fire after adding MITS/EG, which provided valuable time for fire escape and rescue and improved the safety of evacuation.

Figure 6 h exhibits the mass change curve during the cone calorimeter test. The mass of the pure sample decreased rapidly after ignition, reaching the final mass (8.33 wt% at about 70 s and the mass-loss rate (MLR) was 4.41 g/s·m^{-2}. After adding 20 wt% MITS, the MLR of RPUF-2 decreased (3.72 g/s·m^{-2}) and the final char residue increased to 11.17 wt%. When 20

wt% MITS/EG was added, the MLR of RPUF-4 was significantly reduced, which was 49.66% lower than that of the pure sample, and the final residual char content was increased to 23.32 wt%, indicating that MITS/EG system could effectively improve the high-temperature stability of the composites.

The flame retardancy index (FRI) is a dimensionless factor that characterizes the flame retardant properties of composites by PHRR, THR and TTI. FRI is defined as the dimensionless ratio between $THR * \left(\frac{PHRR}{TTI}\right)$, where the molecular term corresponds to the neat polymer, and the denominator term corresponds to the composite [38]:

$$FRI = \frac{\left[THR * \left(\frac{PHRR}{TTI}\right)\right]_{NeatPolymer}}{\left[THR * \left(\frac{PHRR}{TTI}\right)\right]_{Composite}} \qquad (3)$$

The fame retardancy of composites can be qualitatively expressed using the FRI, with three possible cases, 'Poor' (FRI < 1), 'Good' (FRI < 10), and 'Excellent' ($10 < FRI < 10^2$), defined on a logarithmic scale (Table 6). The table indicated that the FRI values of RPUF-2, RPUF-4 and RPUF-6 were greater than 1 after the addition of MITS and/or EG, indicating that MITS and/or EG enhanced the flame retardant properties of FR-RPUF. In addition, the FRI values in some other articles are calculated and summarized in Table 6, from which it could be found that RPUF-4 maintains excellent flame retardant properties.

Figure 7 presents photographs of char residue after the cone calorimeter test of RPUF and FR-RPUF composites. Figure 7 a shows that the surface of the char layer of the pure sample was loose and easy to rupture, which was not conducive to blocking the transport of oxygen and material, so the flame retardancy of pure RPUF was poor. After adding 20

Figure 7 Photographs of char residue after cone calorimetry of RPUF and FR-RPUF composites: **a** RPUF-1; **b** RPUF-2; **c** RPUF-4; **d** RPUF-6.
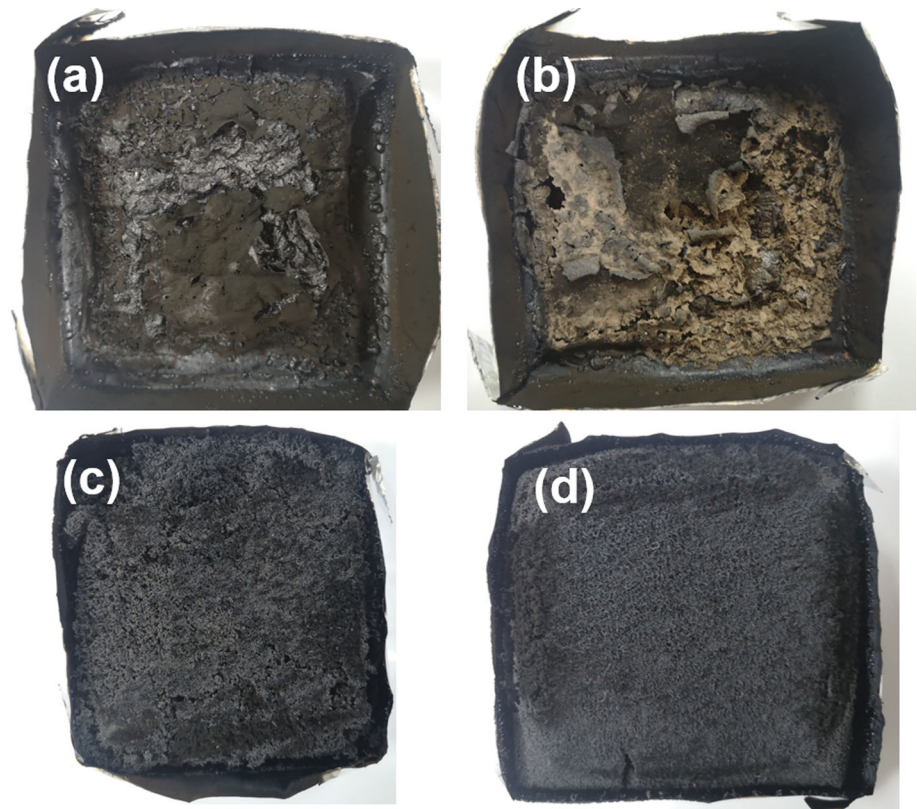
wt% MITS, the char layer of RPUF-2 was damaged more seriously, and the brown inorganic metal oxides were distributed on the surface, indicating that the addition of MITS alone could not promote the formation of a dense char layer of RPUF. When 20 wt% EG or MITS/EG was added, obvious worm-like structures were observed on the surface of char layers of RPUF-4 and RPUF-6, which could play a role in condensed phase flame retardant and effectively improve the fire safety of composites.

Gaseous product

TG-FTIR was used to investigate the effect of the MITS/EG system on the release strength of the cracked gas products of the composites [42]. The FTIR spectra of RPUF and FR-RPUF gas products at the maximum degradation rate are displayed in Fig. 8. The infrared peak values of the four materials were basically the same, implying that MITS/EG did not change the degradation mechanism of RPUF composites, and the gas products were still mainly hydrocarbons, isocyanates [43], aromatic compounds, CO_2, carbonyl compounds, and esters [44].
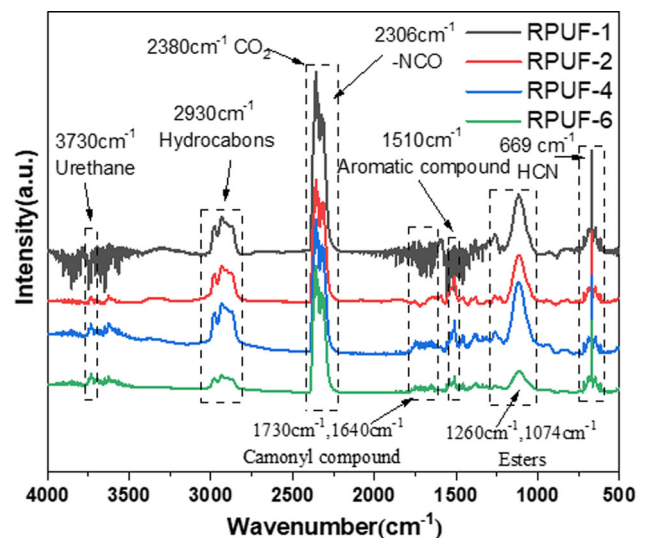

Figure 8 TG-FTIR spectra of pyrolysis products at a maximal decomposition rate of RPUF and FR-RPUF composites.

Figure 9 is the typical gas-phase product release strength curve of RPUF and FR-RPUF composites. It can be observed from Fig. 9a that the G-S curves of RPUF-2, RPUF-4 and RPUF-6 were lower than those of pure samples, and the curve of RPUF-4 was lower than that of RPUF-6, indicating that MITS could
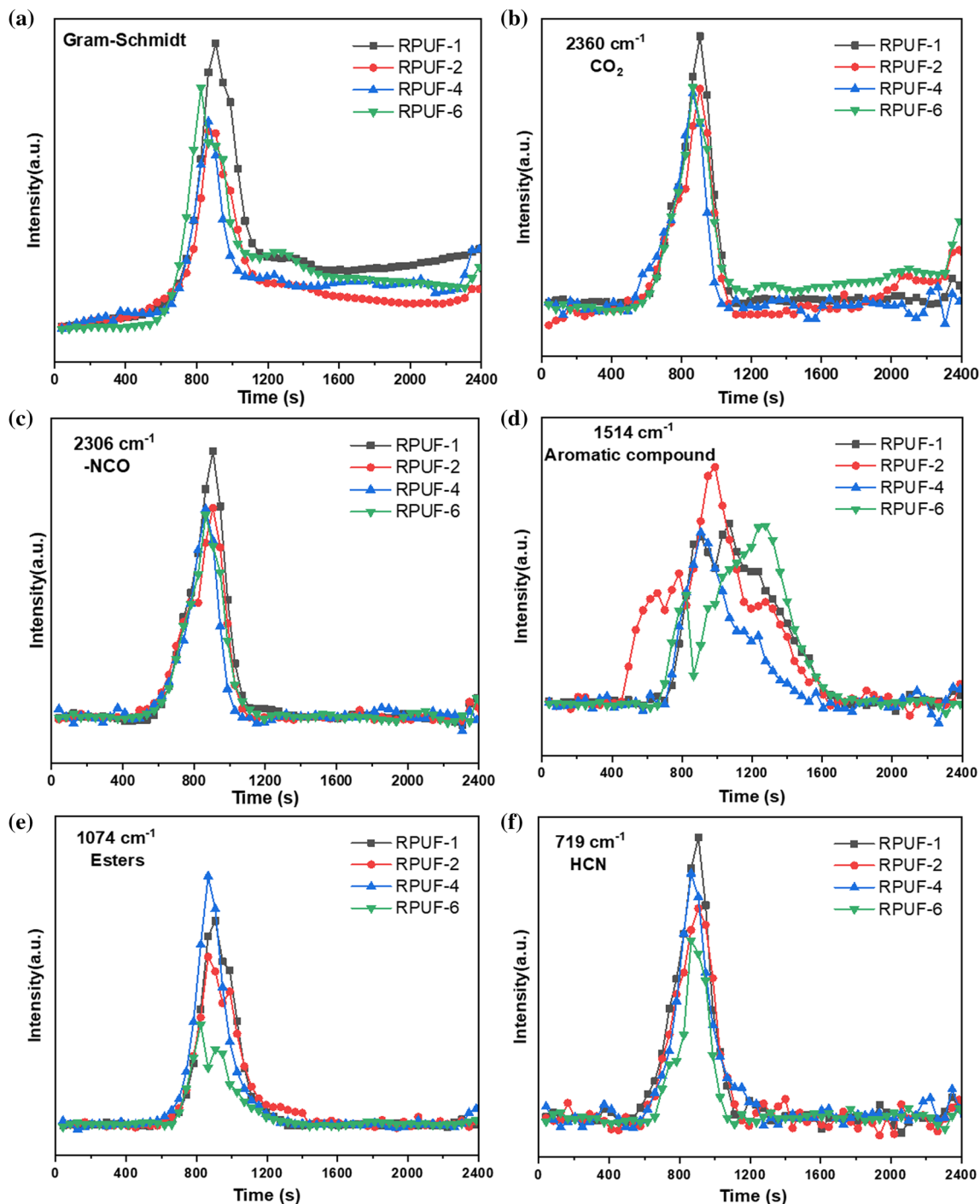
Figure 9 Absorbance of pyrolysis products of RPUF and FR-RPUF versus time: **a** Gram–Schmidt; **b** CO_2; **c** isocyanate compound; **d** aromatic compounds; **e** esters; **f** HCN.

effectively inhibit the pyrolysis of polyurethane matrix and reduce the formation of its gaseous products. Figure 9b, c, and f shows the release curves of CO_2, isocyanates and HCN, respectively. It could be seen that MITS, EG and MITS/EG systems reduce

the release intensity of CO_2, isocyanates and HCN during the pyrolysis of composites. Figure 9d exhibits the release curve of aromatic compounds. Pure RPUF was a bimodal structure that appears around 900 and 1100 s, respectively. The release intensity of

RPUF-2 is higher than that of the pure sample and the peak time of RPUF-2 and RPUF-4 was earlier than that of the pure sample, while the peak time of RPUF-6 was delayed. The peak intensities of RPUF-4 and RPUF-6 were almost the same as those of the pure sample, indicating that MITS/EG system had a certain inhibitory effect on the generation of aromatic compounds. Figure 9e shows the release curves of esters. As shown in the figure, the addition of MITS and EG inhibited the formation of esters, but the MITS/EG system promoted the formation of esters.

Overall, the total pyrolysis products of RPUF-2 and RPUF-4 were lower than those of pure samples, indicating that MITS and MITS/EG reduced the release intensity of gaseous products and reduced the release of toxic and combustible gases.

Char residue analysis

The morphology of char residue for RPUF and FR-RPUF composite is shown in Fig. 10. It can be seen from Fig. 10a, a1 that the char residue of RPUF was loose, thin, and easy to break. Such a structure was

Figure 10 SEM images of char residues for RPUF and FR-RPUF composites: **a**: RPUF-1; **b**: RPUF-2; **c**: RPUF-4; **d**: RPUF-6.
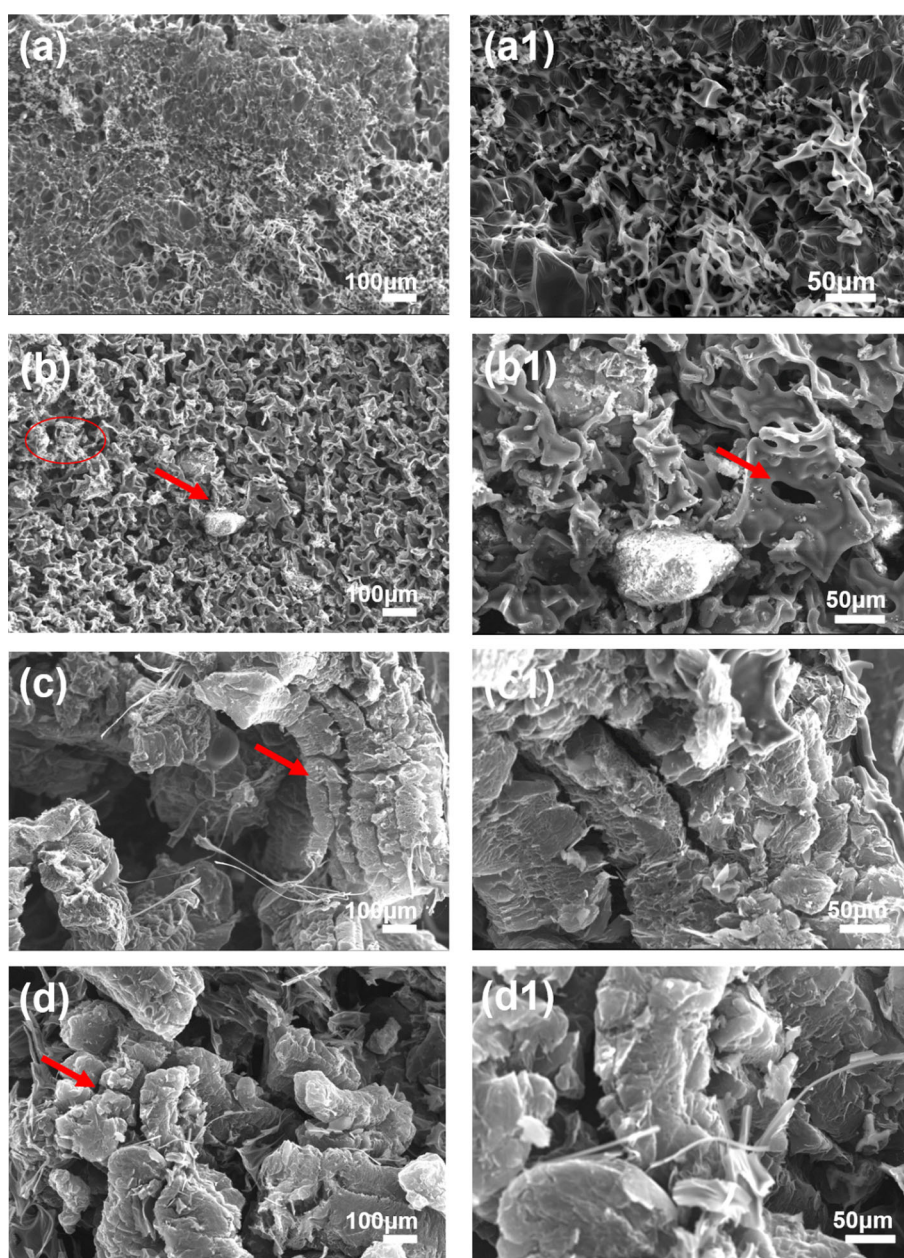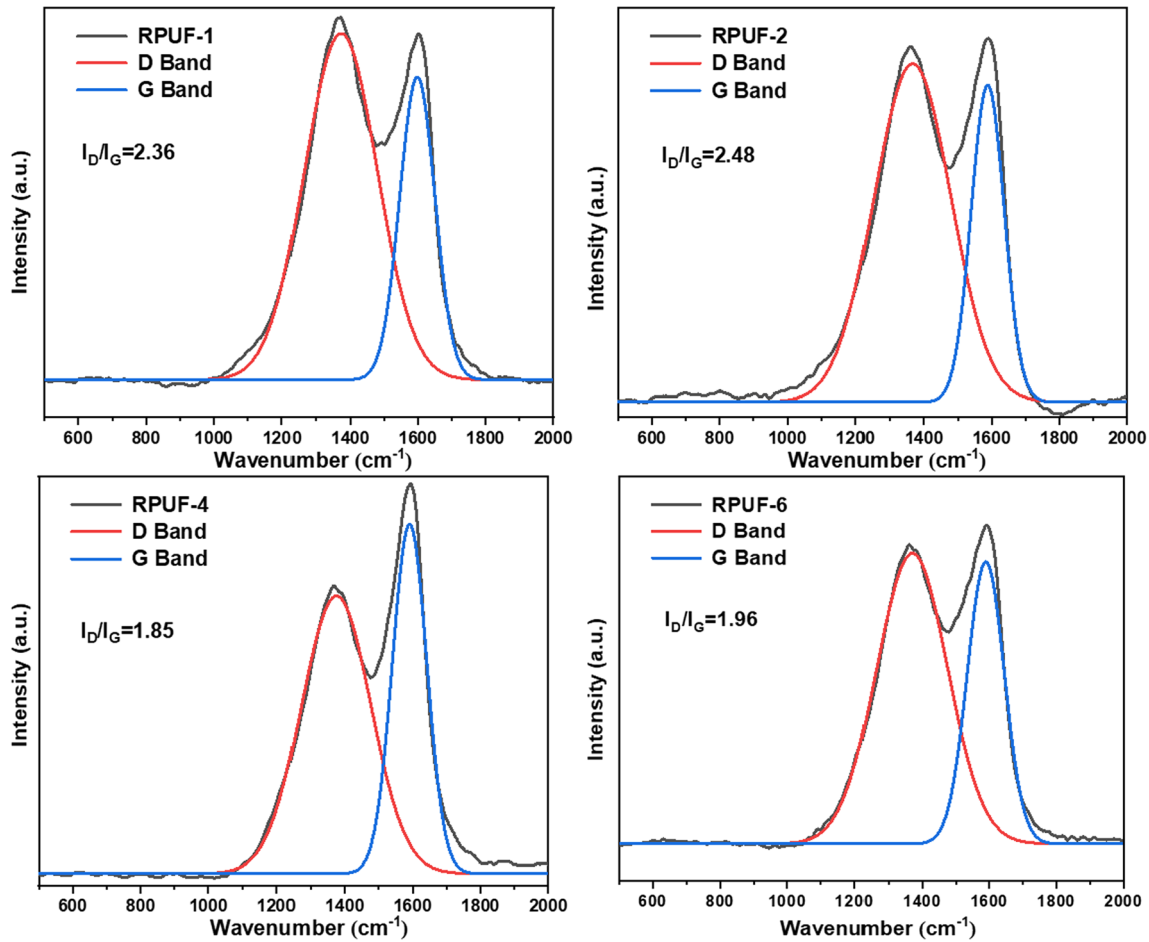
Figure 11 Raman spectra of char residue for RPUF and FR-RPUF composites.

not conducive to preventing the spread of flame and heat and mass transfer, resulting in a low limiting oxygen index. When 20 wt% MITS was added, the thickness of the char layer for RPUF-2 increased slightly, but the pores penetrated through the char layer surface and MITS particles could be obviously observed on the char layer surface. When 20 wt% EG was added, the worm-like structure of EG after combustion expansion can be obviously observed in Fig. 10d, d1 [45], which effectively prevented heat and mass transfer during combustion. Figure 10c, c1 also observes a worm-like structure and the size of the worm-like char layer was larger than RPUF-6, indicating that MITS promoted EG expansion, while MITS mixed with expanded char layer effectively improved the heat resistance of the char layer, thereby protecting the underlying material to achieve the purpose of flame retardant.

Raman spectra of RPUF and FR-RPUF composites are analyzed to understand the effect of the MITS/EG system on the char formation ability of the RPUF matrix. As shown in Fig. 11, all curves show two characteristic peaks, corresponding to the D peak of amorphous carbon SP^3 vibration (1360 cm^{-1}) and the G peak of SP^2 vibration with complete graphitization structure (1580 cm^{-1}) [33, 46], respectively. The graphitization degree of the material is expressed by the area ratio of D peak to G peak (I_D/I_G) [47–49]. The smaller I_D/I_G is, the higher the graphitization degree of the formed char slag is and the better heat resistance of the char slag is [38], so it effectively plays the role of condensed phase flame retardant. The I_D/I_G of the pure sample was 2.36, while the I_D/I_G of RPUF-2 increased to 2.48 when 20 wt% MITS was added, which was mainly due to the poor catalytic ability of MITS which was mainly metal oxides alone. When 20 wt% EG was added, the I_D/I_G of RPUF-6 decreased to 1.96, indicating that EG promoted the formation of the graphitization char layer. When 20 wt% MITS/EG was added, the Ii_D/I_G of RPUF-4 further decreased to 1.85,
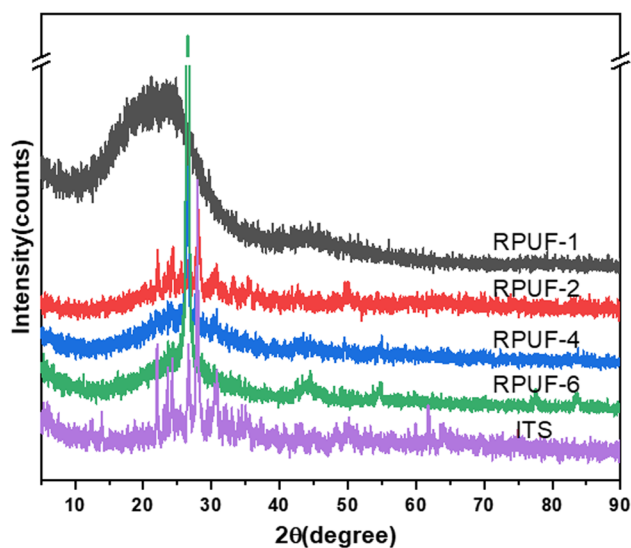
Figure 12 XRD spectra of char residue for RPUF and FR-RPUF composites.

Figure 13 XPS spectra of char residues for RPUF and FR-RPUF composites.

indicating that MITS/EG system could effectively improve the graphitization degree of the char layer, which was mainly because MITS reacted with EG and RPUF pyrolysis products to form metal ions-carbon compound char layer compounds.

In order to understand the existence of ITS in the char residue, the char residue of RPUF and FR-RPUF composites was analyzed by XRD. As exhibited in Fig. 12, a wide peak appeared in the pure sample at $2\theta = 23°$, which was caused by amorphous char formed by RPUF combustion [50]. When 20 wt% EG was added, RPUF-6 showed a sharp peak at $2\theta = 26.44°$, corresponding to the (002) crystal plane of EG [51, 52]. When 20 wt% MITS was added to RPUF-2, some characteristic peaks of ITS disappeared, and the remaining peak area decreased significantly, indicating that there was a certain chemical reaction between MITS and RPUF pyrolysis products. When 20 wt% MITS/EG was added, most of the characteristic peaks of ITS in the XRD curve of RPUF-4 disappeared, and only two obvious peaks at $2\theta = 26°$ and $27°$ still existed, which were the characteristic peaks of EG and ITS, respectively.

In order to further understand the main elements in the char residue and their bonding state, XPS test was performed on the composites and the results are shown in Fig. 13. It could be seen that the char residue of the RPUF mainly contained C, N and O, and the contents were 67.39, 14.21 and 18.4%, respectively. After adding MITS, the content of C and N in the char residue for RPUF-2 decreased, and the
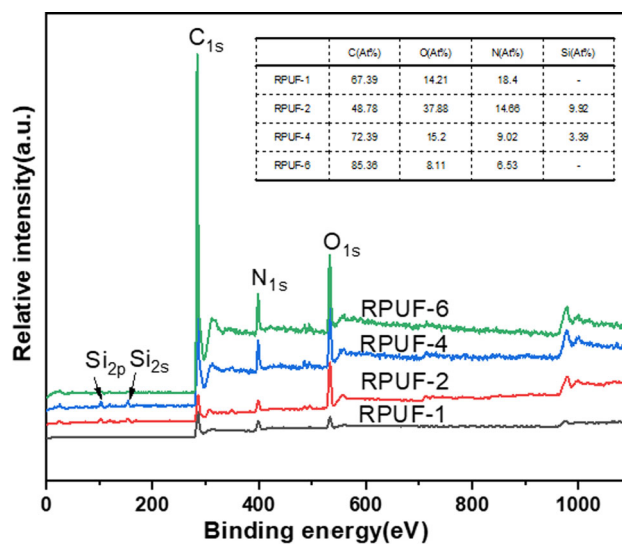
content of O increased. In addition, it also contained 9.92% Si element. Due to the introduction of EG into RPUF-4 and RPUF-6, the C element of the composites increased significantly and the N element decreased.

XPS PEAK41 software was used to perform peak fitting for the main elements C, N and O in the char residues to understand the binding state of the main elements, and the fitting results are shown in Table 7. Figure 14 shows the C (1 s) peak fitting spectra of char residues for RPUF and FR-RPUF composites. The peak at 284.7 eV represented the C element existing in the C–C or C–H bond in the char residues, which corresponded to the graphite carbon structure in the char residues. The peak at 285.5 eV represented C in the form of C–O or C–N bond, which was mainly corresponding to the structures of esters, ethers, alcohols, and phenols on the surface of carbon layer. The peak at 287.4 eV represented C in the form of C = O or C = N, corresponding to the char residue's surface with carbonyl, carboxylic acid (salt), ester group, aromatic heterocyclic compounds and other structures [53]. The C content in RPUF with medium C–C/C–H, C–O/C–N and C=O/C=N structure was 44.54%, 26.81% and 28.94%, respectively. The addition of MITS resulted in a significant increase in the C–O/C–N content of RPUF-2, and the addition of EG and MITS/EG resulted in a significant increase in the C–C/C–H content, indicating that EG can contribute to a more regular and dense char residue.

Figure 15 shows the O (1 s) peak fitting spectra of char residues for RPUF and FR-RPUF composites.

Table 7 Bonding state data of C, N, O in char residue of RPUF and FR-RPUF composites

Sample	C			O			N	
	C–C/C–H 284.7 eV/%	C–O/C–N 285.5 eV/%	C = O/C = N 287.4 eV/%	= O 531.3 eV/%	–O– 532.5 eV/%	O_2/H_2O 533.7 eV/%	–NH– 398.8 eV/%	= N 400.4 eV/%
RPUF-1	44.54	26.81	28.64	49.11	19.38	31.51	54.79	45.21
RPUF-2	40.34	41.72	17.94	42.98	40.94	16.08	60.56	39.44
RPUF-4	53.42	20.90	25.68	60.94	17.12	21.93	58.86	41.14
RPUF-6	57.47	20.05	22.45	53.76	35.50	10.74	62.73	37.27
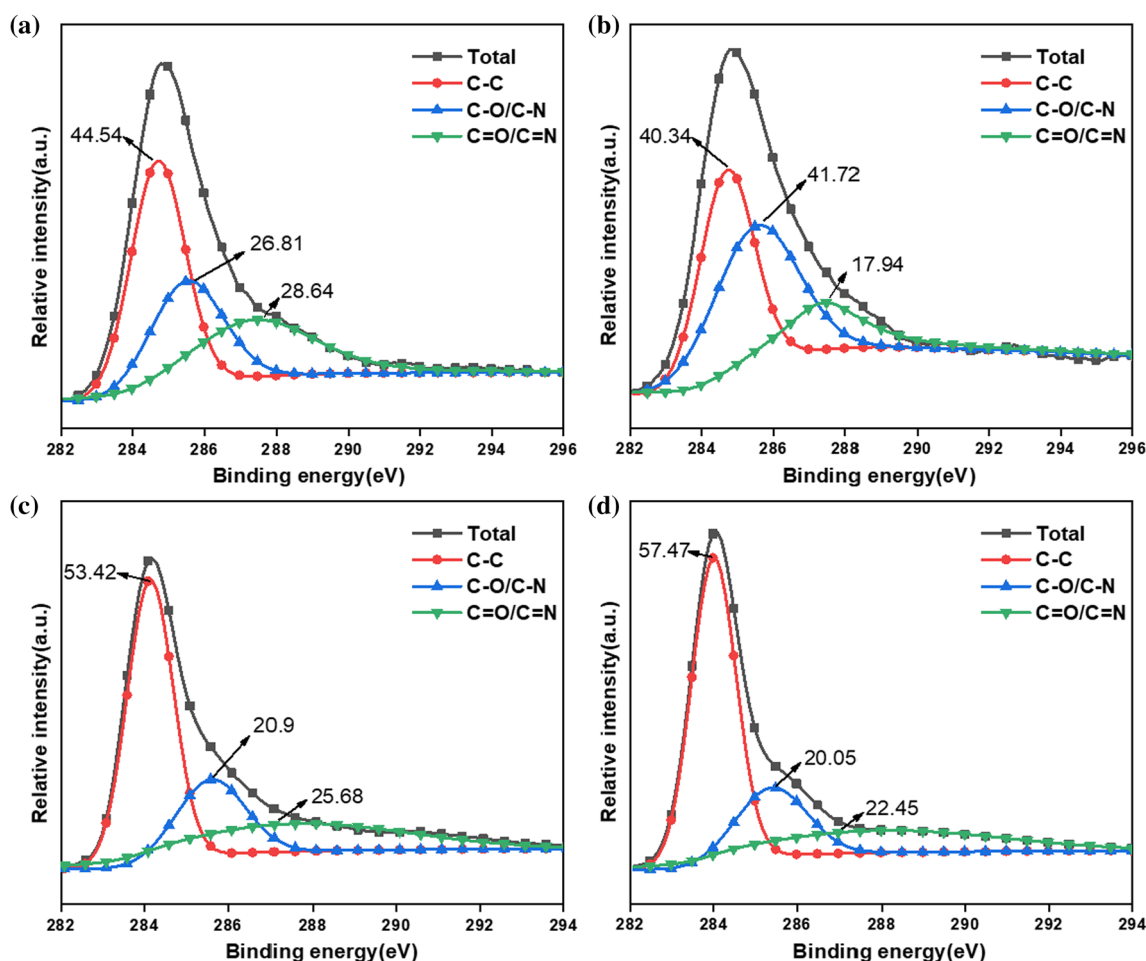
Figure 14 C1s spectra of char residue for RPUF and FR-RPUF composites: **a** RPUF-1; **b** RPUF-2; **c** RPUF-4; **d** RPUF-6.

The peak at 531.3 eV corresponded to the = O structure of carbonyl, quinone, carboxylic acid (salt) and ester in char residue, the peak at 532.5 eV corresponded to the –O–structure in the form of alcohol, ether and phenol, and the peak at 533.7 eV corresponded to the O element in the form of adsorbed oxygen (O_2) and free water (H_2O) [54]. The structures of = O, – O – and O_2/H_2O in RPUF accounted for 49.11, 19.38, and 31.51%, respectively. With the addition of MITS, the O element of RPUF-2 mainly as – O – structure, and its proportion increased to 40.94%. The proportion of O_2/H_2O structure decreased to 16.08%. When EG was added, the proportion of=O structure in char residue for RPUF-6 increased slightly, and the content of O element in – O – form increased to 35.5%. When MITS/EG
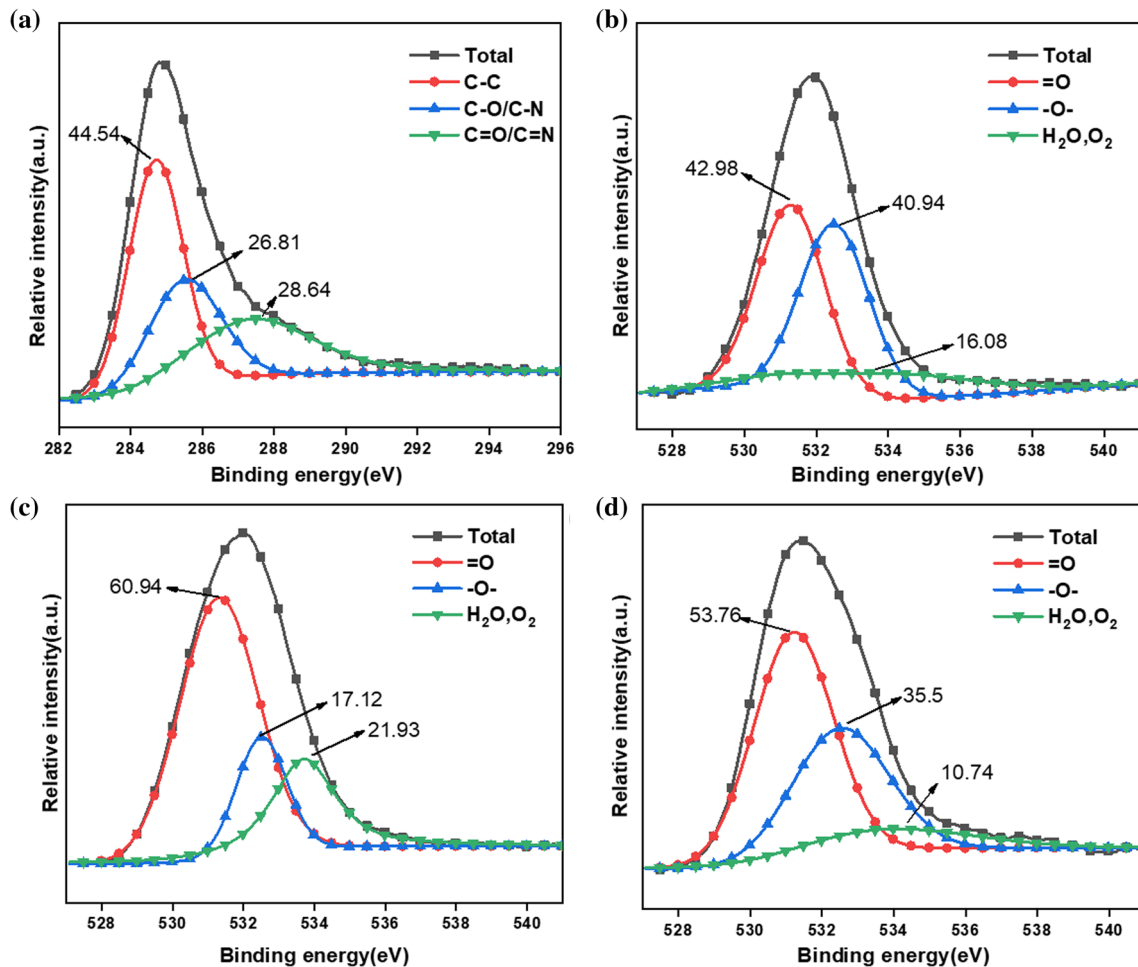
Figure 15 O1s spectra of char residue for RPUF and FR-RPUF composites: **a** RPUF-1; **b** RPUF-2; **c** RPUF-4; **d** RPUF-6.

was added, the O element of RPUF-4 mainly existed in the form of $=O$, indicating that the compactness of char residue was significantly improved and MITS/EG changed the bonding state of O element in char residue.

Figure 16 shows the N (1 s) peak fitting spectra of char residues for RPUF and FR-RPUF composites. The peak at 398.8 eV corresponded to the N element in the amide and amine compounds with the $-NH-$ structure in the char residues, and the peak at 400.4 eV corresponded to the N in aromatic heterocyclic compounds with $=N$ structure. The MITS and/or EG promoted the development of N element in char residues toward $-NH-$ structure.

Figure 17 shows the Si (2p) spectra of char residues for RPUF-2 and RPUF-4 composites. It can be seen from the figure that RPUF-2 had a peak at about 103 eV, indicating the presence of SiO_2 in char

residue [55], while RPUF-4 had a higher peak intensity, indicating that EG promotes the formation of SiO_2.

Flame retardant mechanism

Based on the above analysis, the flame retardant mechanism of RPUF/MITS/EG composites was proposed. As shown in Fig. 18, the oxide in MIT improved the thermal stability of RPUF composites in the early stage of combustion. When RPUF/MITS/EG composites are heated, acidic substances such as sulfuric acid and nitric acid in EG particles decompose and release a large number of acidic gases during combustion, which promotes the degradation of hard segments of rigid polyurethane foam and the formation of wormlike char layers as gas sources. The metal oxide in MIT played its role by catalytic
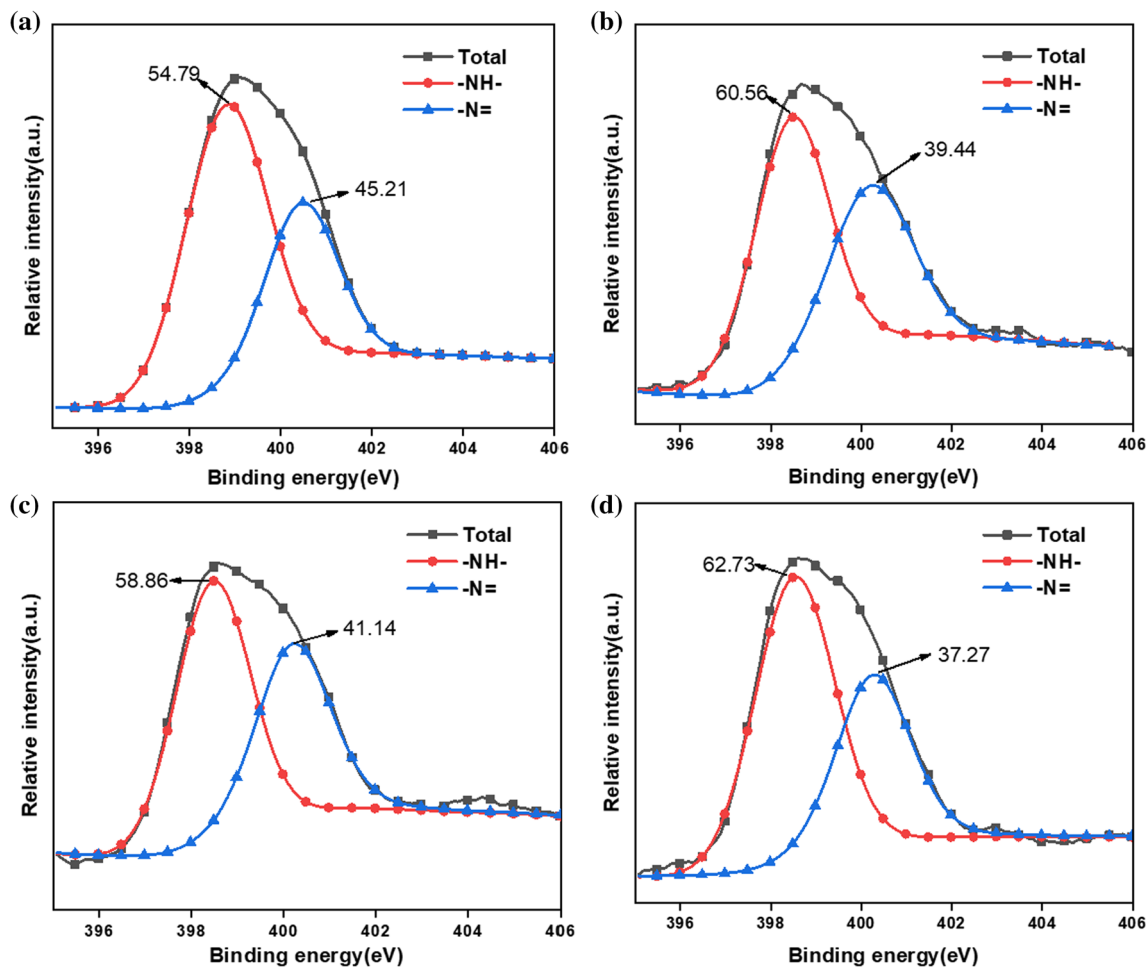
Figure 16 N1s spectra of char residue for RPUF and FR-RPUF composites: a RPUF-1; b RPUF-2; c RPUF-4; d RPUF-6.
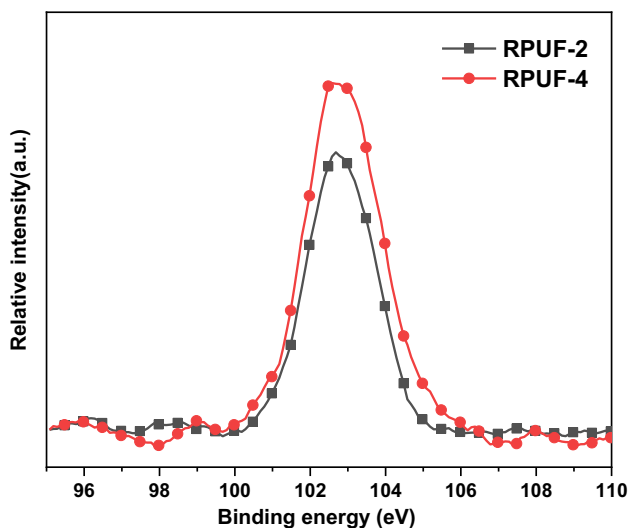

Figure 17 Si2p spectra of char residue for RPUF-2 and RPUF-4 composites.

carbonization effect and can promote the char formation of RPUF composites, and the acidic substances in EG react with metal oxides to form a metal ion carbon layer. The SiO_2 produced by the MITS and decomposition of KH550 and the unreacted metal/non-metal oxides are distributed in the worm-like char layer to enhance the condensed phase flame retardant effect. Therefore, MITS/EG mainly plays a condensed phase flame retardant role.

Conclusion

In this paper, modified iron tailings (MITS) were prepared by surface modification of iron tailings (ITS) with KH550, and the synergistic system of MITS/EG flame retardant rigid polyurethane foam (RPUF) was composed of expandable graphite (EG). The effects of a synergistic system on the thermal stability of RPUF matrix and gas-phase products were systematically

Figure 18 Schematic illustration for the flame retardant mechanism of FR-RPUF composites.
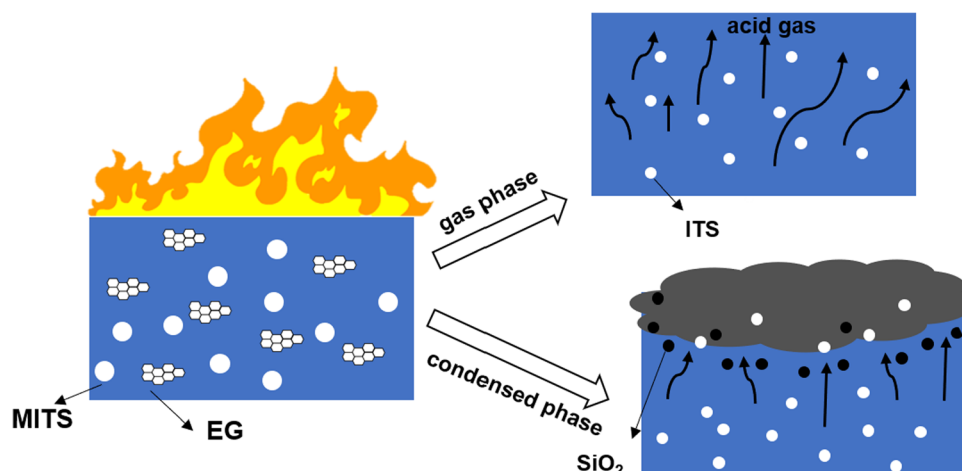
studied. TG test showed that when 20 wt% EG/MITS was added, the $T_{-50\ wt\%}$, T_{max1}, and T_{max2} of RPUF-4 were increased to 386, 334, and 486 °C, respectively. The char residue at 700 °C is 35.76 wt%, which is 82.82% higher than that of the pure sample, indicating that the combination of EG and MITS can effectively improve the high-temperature stability of the composites. The CCT test showed that MITS/EG promoted the formation of a dense carbon layer, thereby reducing the thermal and non-thermal hazards of composites. The PHRR, TSR, and SF of RPUF-4 were reduced by 61.55, 77.99, and 91.54%, respectively, compared with the pure sample. TG-FTIR test showed that the release intensity of G–S, CO_2, isocyanate compounds, and HCN of RPUF-4 was lower than that of the pure sample after adding MITS/AHP. SEM, Raman and XRD tests show that the synergistic effect of EG and MITS improves the graphitization degree of the carbon slag of the composite.

Acknowledgements

Funding

Declarations

Conflict of interest The author(s) declared no potential conflicts of interest with respect to the research, authorship, and/or publication of this article.

References

[1] Xu ZB, Kong WW, Zhou MX, Peng M (2010) Effect of surface modification of montmorillonite on the properties of rigid polyurethane foam composites. Chin J Polym Sci 28:615–624. https://doi.org/10.1007/s10118-010-9111-0

[2] Zhang JY, Liu BW, Wang YZ, Zhao HB (2022) Recent advances in halogen-free flame-retardant polyurethane foams. Acta Polym Sin 53:842–855

[3] Yang H, Wang X, Song L, Yu B, Yuan Y, Hu Y, Yuen R (2015) Aluminum hypophosphite in combination with expandable graphite as a novel flame retardant system for rigid polyurethane foams. Polym Adv Technol 25:1034–1043. https://doi.org/10.1002/pat.3348

[4] Zhu MH, Ma ZW, Liu L, Zhang JZ, Huo SQ, Song PA (2022) Recent advances in fire-retardant rigid polyurethane foam. J Mater Sci Technol. https://doi.org/10.1016/j.jmst.2021.09.062

[5] Liu BW, Zhao HB, Wang YZ (2022) Advanced flame-retardant methods for polymeric materials. Adv Mater. https://doi.org/10.1002/adma.202107905

[6] Xu W, Liu L, Wang S, Hu Y (2015) Synergistic effect of expandable graphite and aluminum hypophosphite on flame-

retardant properties of rigid polyurethane foam. J Appl Polym Sci 132:42842. https://doi.org/10.1002/app.42842

[7] Bian X, Tang J, Li Z, Lu Z, Lu A (2007) Dependence of flame-retardant properties on density of expandable graphite filled rigid polyurethane foam. J Appl Polym Sci 104:3347–3355. https://doi.org/10.1002/app.25933

[8] Wang S, Qian L, Xin F (2018) The synergistic flame-retardant behaviors of Pentaerythritol phosphate and expandable graphite in rigid polyurethane foams. Polym Compos 39:329–336. https://doi.org/10.1002/pc.23939

[9] Xi W, Qian L, Huang Z, Cao Y, Li L (2016) Continuous flame-retardant actions of two phosphate esters with expandable graphite in rigid polyurethane foams. Polym Degrad Stab 130:97–102. https://doi.org/10.1016/j.polymdegradstab.2016.06.003

[10] Hu X, Wang D (2013) Enhanced fire behavior of rigid polyurethane foam by intumescent flame retardants. J Appl Polym Sci 129:238–246. https://doi.org/10.1002/app.38722

[11] Yao W, Zhang D, Zhang Y, Fu T, Guan D, Dou Y (2019) Synergistic flame retardant effects of expandable graphite and ammonium polyphosphate in water-blow polyurethane foam. Adv Mater Sci Eng 2019:1–8. https://doi.org/10.1155/2019/6921474

[12] Ma ZL, Fan CR, Lu GY, Liu XY, Zhang H (2012) Synergy of magnesium and calcium oxides in intumescent flame-retarded polypropylene. J Appl Polym Sci 125:3567–3574. https://doi.org/10.1002/app.36227

[13] Li X, Zhang K, Shi R, Ma X, Tan L, Ji Q, Xia Y (2017) Enhanced flame-retardant properties of cellulose fibers by incorporation of acid-resistant magnesium-oxide microcapsules. Carbohyd Polym 176:246–256. https://doi.org/10.1016/j.carbpol.2017.08.096

[14] Ping W (2003) An investigation on synergism of an intumescent flame retardant based on silica and alumina. J Fire Sci 21:17–28. https://doi.org/10.1177/0734904103021001002

[15] Chen X, Li M, Zhuo J, Ma C, Jiao C (2016) Influence of Fe_2O_3 on smoke suppression and thermal degradation properties in intumescent flame retardant silicone rubber. J Therm Anal Calorim 123:439–448. https://doi.org/10.1007/s10973-015-4911-7

[16] Yuan B, Chen G, Zou Y, Shang S, Sun Y, Yu B, He S, Chen X (2019) Alumina nanoflake-coated graphene nanohybrid as a novel flame retardant filler for polypropylene. Polym Adv Technol 30:2153–2158. https://doi.org/10.1002/pat.4689

[17] Li Y, Tian X, He X, Liu Y, Ye J, Wei Y (2020) Comprehensive reutilization of iron in iron ore tailings: preparation and characterization of magnetic flocculants. Environ Sci Pollut Res 27:37011–37021. https://doi.org/10.1007/s11356-020-09742-9

[18] Wang S, Peng X, Geng J, Li B, Wang K (2014) Synthesis of calcium silicate hydrate based on steel slag with various alkalinities. J Wuhan Univ Technol 29:789–794. https://doi.org/10.1007/s11595-014-0998-0

[19] Lu C, Yang H, Wang J, Tan Q, Fu L (2020) Utilization of iron tailings to prepare high-surface area mesoporous silica materials. Sci Total Environ 736:139483. https://doi.org/10.1016/j.scitotenv.2020.139483

[20] Santander M, Valderrama L (2019) Recovery of pyrite from copper tailings by flotation. J Mater Res Technol 8:4312–4317. https://doi.org/10.1016/j.jmrt.2019.07.041

[21] Tao Y, Li P, Cai L, Shi SQ (2019) Flammability and mechanical properties of composites fabricated with CaCO3-filled pine flakes and Phenol Formaldehyde resin. Compos Part B Eng 167:1–6. https://doi.org/10.1016/j.compositesb.2018.12.005

[22] Lei M, Tang L, Du H, Peng L, Tie B, Williams PN, Sun GX (2019) Safety assessment and application of iron and manganese ore tailings for the remediation of As-contaminated soil. Process Saf Environ 125:334–341. https://doi.org/10.1016/j.psep.2019.01.011

[23] Yang R, Wang B, Han X, Ma B, Li J (2017) Synthesis and characterization of flame retardant rigid polyurethane foam based on a reactive flame retardant containing phosphazene and cyclophosphonate. Polym Degrad Stab 144:62–69. https://doi.org/10.1016/j.polymdegradstab.2017.08.008

[24] Harpal S (2016) Rigid polyurethane foam: a versatile energy efficient material. Key Eng Mater 678:88–98. https://doi.org/10.4028/www.scientific.net/KEM.678.88

[25] Zhang M, Luo Z, Zhang J, Chen S, Zhou Y (2015) Effects of a novel phosphorus-nitrogen flame retardant on rosin-based rigid polyurethane foams. Polym Degrad Stab 120:427–434. https://doi.org/10.1016/j.polymdegradstab.2015.08.001

[26] Zheng X, Wang G, Xu W (2014) Roles of organically-modified montmorillonite and phosphorous flame retardant during the combustion of rigid polyurethane foam. Polym Degrad Stab 101:32–39. https://doi.org/10.1016/j.polymdegradstab.2014.01.015

[27] Cao Z, Liao W, Wang S, Zhao H, Wang Y (2019) Polyurethane foams with functionalized graphene towards high fire-resistance, low smoke release, superior thermal insulation. Chem Eng J 361:1245–1254. https://doi.org/10.1016/j.cej.2018.12.176

[28] Wang X, Hu Y, Song L, Xing W, Lu H (2010) Thermal degradation behaviors of epoxy resin/POSS hybrids and phosphorus-silicon synergism of flame retardancy. J Polym Sci B Polym Phys 48:693–705. https://doi.org/10.1002/polb.21939

[29] Li M, Wang S, Han L, Yuan W, Cheng J, Zhang A, Zhao H, Wang Y (2019) Hierarchically porous SiO_2/polyurethane

foam composites towards excellent thermal insulating, flame-retardant and smoke-suppressant performances. J Hazard Mater 375:61–69. https://doi.org/10.1016/j.jhazmat.2019.04.065

[30] Bernhard S, Charles AW, Giovanni C (2016) Recommendations on the scientific approach to polymer flame retardancy: part 1–Scientific terms and methods. J Fire Sci 34:447–467. https://doi.org/10.1177/0734904116675881

[31] Wu N, Niu F, Lang W, Yu J, Fu G (2019) Synthesis of reactive phenylphosphoryl glycol ether oligomer and improved flame retardancy and mechanical property of modified rigid polyurethane foams. Mater Design 181:107929. https://doi.org/10.1016/j.matdes.2019.107929

[32] Bernhard S, Charles AW, Giovanni C (2017) Recommendations on the scientific approach to polymer flame retardancy: part 2-concepts. J Fire Sci 35:3–20. https://doi.org/10.1177/0734904116675370

[33] Ma ZW, Zhang JZ, Liu L, Zheng H, Dai JF, Tang LC, Song PA (2022) A highly fire-retardant rigid polyurethane foam capable of fire-warning. Compos Commun 29:101046. https://doi.org/10.1016/j.coco.2021.101046

[34] Jiao C, Wang H, Li S, Chen X (2017) Fire hazard reduction of hollow glass microspheres in thermoplastic polyurethane composites. J Hazard Mater 332:176–184. https://doi.org/10.1016/j.jhazmat.2017.02.019

[35] Ma ZW, Liu XC, Xu XD, Liu L, Yu B, Maluk C, Huang GB, Wang H, Song PA (2021) Bioinspired, highly adhesive, nanostructured polymeric coatings for Superhydrophobic fire-extinguishing thermal insulation foam. ACS Nano 15:11667–11680. https://doi.org/10.1021/acsnano.1c02254

[36] Zhu H, Xu S (2019) Synthesis and properties of rigid polyurethane foams synthesized from modified urea-formaldehyde resin. Constr Build Mater 202:718–726. https://doi.org/10.1016/j.conbuildmat.2019.01.035

[37] Zhou Q, Liu C, Zhou K, Xuan X, Shi C (2019) Synergistic effect between solid wastes and intumescent flame retardant on flammability and smoke suppression of thermoplastic polyurethane composites. Polym Adv Technol 31:4–14. https://doi.org/10.1002/pat.4742

[38] Zhu KY, Jiang ZL, Xu XT, Zhang Y, Zhu M, Wang JH, Ren A (2022) Preparation and thermal cross-linking mechanism of co-polyester fiber with flame retardancy and anti-dripping by in situ polymerization. RSC Adv 12:168–180. https://doi.org/10.1039/D1RA07410E

[39] Liu MR, Feng ZH, Zhao RQ, Wang BB, Deng D, Zhou ZJ, Yang YD, Liu XL, Liu XY, Tang G (2022) Enhancement of fire performance for rigid polyurethane foam composites by incorporation of aluminum hypophosphite and expanded graphite. Polym Bull. https://doi.org/10.1007/s00289-022-04084-7

[40] Zhang B, Yang SJ, Liu MR, Wen PY, Liu XY, Tang G, Xu XR (2022) Bio-based trivalent phytate: a novel strategy for enhancing fire performance of rigid polyurethane foam composites. J Renew Mater 10:1201–1220

[41] Tang G, Liu XL, Yang YD, Chen DP, Zhang H, Zhou L, Zhang P, Jiang HH, Deng D (2020) Phosphorus-containing silane modified steel slag waste to reduce fire hazards of rigid polyurethane foams. Adv Powder Technol 31:1420–1430. https://doi.org/10.1016/j.apt.2020.01.019

[42] Cai W, Wang B, Liu L, Zhou X, Chu F, Zhan J, Hu Y, Kan Y, Wang X (2019) An operable platform towards functionalization of chemically inert boron nitride nanosheets for flame retardancy and toxic gas suppression of thermoplastic polyurethane. Compos Part B-Eng 178:107462. https://doi.org/10.1016/j.compositesb.2019.107462

[43] Yang S, Zhang B, Liu M, Yang Y, Liu X, Chen D, Wang B, Tang G, Liu X (2021) Fire performance of piperazine phytate modified rigid polyurethane foam composites. Polym Adv Technol 32:4531–4546. https://doi.org/10.1002/pat.5454

[44] Tang G, Zhou L, Zhang P, Han Z, Chen D, Liu X, Zhou Z (2020) Effect of aluminum Diethylphosphinate on flame retardant and thermal properties of rigid polyurethane foam composites. J Therm Anal Calorim 140:625–636. https://doi.org/10.1007/s10973-019-08897-z

[45] Hu Y, Zhou Z, Li S, Yang D, Zhang S, Hou Y (2021) Flame retarded rigid polyurethane foams composites modified by aluminum Diethylphosphinate and expanded graphite. Front Mater 7:629284. https://doi.org/10.3389/fmats.2020.629284

[46] Wang L, Tawiah B, Shi Y, Cai S, Rao X, Liu C, Yang Y, Yang F, Yu B, Liang Y, Fu L (2019) Highly effective flame-retardant rigid polyurethane foams: fabrication and applications in inhibition of coal combustion. Polymers 11:1776. https://doi.org/10.3390/polym11111776

[47] Guo W, Wang X, Huang J, Zhou Y, Cai W, Wang J, Song L, Hu Y (2020) Construction of durable flame-retardant and robust superhydrophobic coatings on cotton fabrics for water-oil separation application. Chem Eng J 398:125661. https://doi.org/10.1016/j.cej.2020.125661

[48] Tang G, Jiang H, Yang Y, Chen D, Liu C, Zhang P, Zhou L, Huang X, Zhang H, Liu X (2020) Preparation of melamine-formaldehyde resin-microencapsulated ammonium polyphosphate and its application in flame retardant rigid polyurethane foam composites. J Polym Res 27:375. https://doi.org/10.1007/s10965-020-02343-7

[49] Wang S, Gao R, Zhou K (2018) The influence of cerium dioxide functionalized reduced graphene oxide on reducing fire hazards of thermoplastic polyurethane nanocomposites. J Colloid Interface Sci 536:127–134. https://doi.org/10.1016/j.jcis.2018.10.052

[50] Ma ZW, Zhang JZ, Maluk C, Yu YM, Seraji SM, Yu B, Wang H, Song PA (2022) A lava-inspired micro/nano-structured ceramifiable organic-inorganic hybrid fire-extinguishing coating. Matter 5:911–932. https://doi.org/10.1016/j.matt.2021.12.009

[51] Cheng Z, Liao D, Hu X, Li W, Xie C, Zhang H, Yang W (2020) Synergistic fire retardant effect between expandable graphite and ferrocene-based non-phosphorus polymer on polypropylene. Polym Degrad Stab 178:109201

[52] Pang X, Shi X, Kang X, Duan M, Weng M (2015) Preparation of borate–modified expandable graphite and its flame retardancy on acrylonitrile-butadiene-styrene resin. Polym Compos 37:2673–2683. https://doi.org/10.1002/pc.23461

[53] Wu S, Deng D, Zhou L, Zhang P (2019) Tang G (2019) Flame retardancy and thermal degradation of rigid polyurethane foams composites based on aluminum hypophosphite. Mater Res Express 6:105362. https://doi.org/10.1088/2053-1591/ab41b2

[54] Tang G, Zhou L, Zhang P, Han ZQ, Chen DP, Liu XY, Zhou ZJ (2019) Effect of aluminum diethylphosphinate on flame retardant and thermal properties of rigid polyurethane foam composites. J Therm Anal Calorim 140:625–636. https://doi.org/10.1007/s10973-019-08897-z

[55] Wu CL, Wang BB, Zheng JQ, Li HX (2018) Flux mechanism of compound flux on ash and slag of coal with high ash melting temperature. Chin J Chem Eng 27:1200–1206. https://doi.org/10.1016/j.cjche.2018.09.006